ACS OMEGA

Open Access

http://pubs.acs.org/journal/acsodf

Article

Study on Sulfuric Acid Condensation on Planar and Particle Surfaces in Flue Gas by Thermodynamic Equilibrium Analysis

Zuozhou Tang, Zhongwei Li, Bingqiang Ji,* and Qiang Song*

Cite This: *ACS Omega* 2025, 10, 19625−19635

Read Online

ACCESS | Metrics & More | Article Recommendations | Supporting Information

ABSTRACT: SO_3 in coal-fired flue gas causes equipment corrosion and sulfuric acid mist emissions. As the flue gas temperature decreases, SO_3 converts to gaseous H_2SO_4 and condenses with H_2O via binary heterogeneous condensation. Here, based on thermodynamic equilibrium theory, a model for H_2SO_4−H_2O binary heterogeneous condensation is developed and verified by comparing the calculated planar acid dew point ($T_{ADP,plane}$) with the previously reported experimental data. The equilibrium parameters of condensation on both planar and particle surfaces are investigated. On planar surface, $T_{ADP,plane}$ increases with the gas concentration, while the equilibrium sulfuric acid mass fraction ($\omega_{PE,plane}$) increases with H_2SO_4 concentration and decreases with H_2O concentration. For H_2SO_4 concentrations of 0.5−50 ppm and H_2O concentrations of 0.5%−15%, $T_{ADP,plane}$ ranges from 356.37 to 426.67 K and the equilibrium sulfuric acid mass fraction ($\omega_{PE,plane}$) ranges from 71.922% to 91.058%. The equilibrium parameters on micrometer particle surfaces are similar to those on planar surfaces, while on submicrometer particle surfaces, the acid dew point ($T_{ADP,particle}$) decreases and the equilibrium liquid film sulfuric acid mass fraction ($\omega_{PE,particle}$) increases with decreasing particle diameter (d_p) due to the Kelvin effect. We found that $T_{ADP,particle}/T_{ADP,plane}$ and $\omega_{PE,particle}/\omega_{PE,plane}$ are barely unaffected by $p_{v,i}$ and can be considered as a function of d_p. Based on the numerical results, formulas with good prediction accuracy for $T_{ADP,particle}$ and $\omega_{PE,particle}$ are proposed. The results provide predictive models for acid dew points on particle surfaces, which are crucial for guiding strategies to mitigate corrosion and reduce sulfuric acid mist emissions in coal-fired power plants.

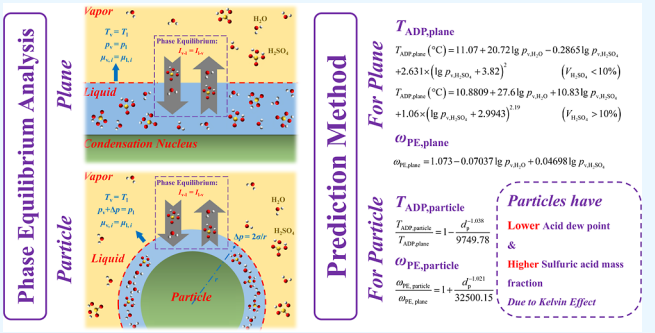

1. INTRODUCTION

The sulfur element in coal is oxidized during combustion forming sulfur oxides (SO_x), which mainly consist of SO_2 and contains about 0.75%−1.5% SO_3.[1,2] After passing through the Selective Catalytic Reduction unit, about 0.5%−2% of SO_2 is oxidized to SO_3 by vanadium-based catalysts.[3−7] Depending on the sulfur content in coal and the performance of the energy-saving and emission-reduction units, the SO_3 content in coal-fired flue gases can range from several to tens of mg/Nm,[3] while the SO_3 content in flue gas from power plants using high-sulfur coal can exceed 100 mg/Nm^3,[3,8] which far exceed the sulfuric acid mist emission standards proposed by developed countries and regions.[2,9]

In the flue gas system, as the flue gas temperature decreases, gaseous SO_3 begins to convert to gaseous H_2SO_4 at approximately 500 °C[10] and then completely transforms into H_2SO_4 at around 205 °C.[11] As the temperature further decreases, gaseous H_2SO_4 begins to undergo binary condensation with H_2O. The condensation process of H_2SO_4−H_2O can be classified into homogeneous condensation and heterogeneous condensation based on whether they adhere to existing condensation nuclei.[12,13] It is reported that homogeneous condensation occurs only when the concentration of the condensable components is high enough and there are few or no existing condensation nuclei.[14,15] In the flue gas system, due to the existence of abundant condensation nuclei provided by the surfaces of heat exchangers and fly ash particles, the condensation of H_2SO_4 with H_2O mainly occurs heterogeneously. The sulfuric acid liquid film formed on the equipment surfaces can cause corrosion, threatening the safety and stable operation of power generation systems.[16] When H_2SO_4 condenses onto fly ash particle surfaces, it may deposit along with the particles onto the equipment surfaces in the flue, leading to corrosion[17−19] or it may be emitted into the atmosphere as sulfuric acid mist, threatening environment and human health.[20,21] Therefore, investigating the H_2SO_4−H_2O binary heterogeneous condensation is of great significance for corrosion prevention and control of acid mist emissions in flue gas systems.

Received: January 14, 2025
Revised: April 10, 2025
Accepted: April 23, 2025
Published: May 5, 2025

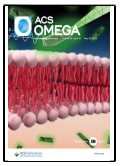

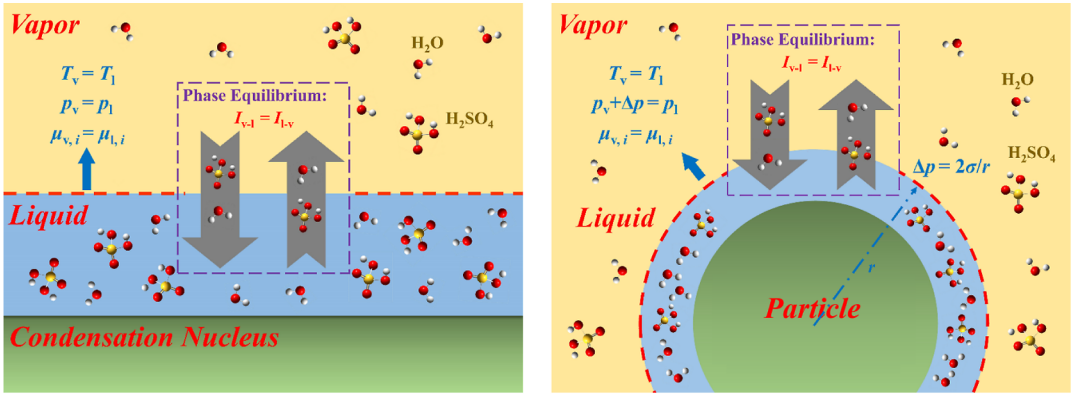

Figure 1. Schematics illustrating the binary equilibrium of H_2SO_4−H_2O at a (a) planar surface and a (b) curved surface.

Previous studies have primarily focused on the binary condensation of H_2SO_4−H_2O on planar surfaces such as heat exchangers, oriented to address the low-temperature corrosion resulting from H_2SO_4 condensation on heat transfer surfaces.[22,23] The temperature at which gaseous H_2SO_4 and H_2O begin to condense is termed the acid dew point. Numerous experimental observations on flue gas acid dew points have been conducted, and various empirical formulas for acid dew point were proposed. Former Soviet scholars obtained the acid dew point by correcting the water dew point considered fuel sulfur content and excess air coefficient.[24] Muller[25,26] and Halstead[27] proposed formulas to solve the acid dew point using condensable component concentration in flue gas as the variable, but their formulas only consider the concentration of SO_3/H_2SO_4 and neglect the influence of gaseous H_2O on the condensation process. The Japan Institute of Electric Power Industry provided formulas for calculating the acid dew point at specific H_2O vapor concentrations of 5%, 10%, and 15%.[24] Haase and Borgmann,[24] Verhoff and Banchero,[28] Bapahoba,[24] and Okkes[29] proposed different formulas for the acid dew point considering both H_2SO_4 and H_2O vapor concentrations. Significant deviations exist between the results calculated using different formulas due to the differences in experimental observation methods and the interpretation of acid condensation signals.[30,31] Among the formulas mentioned above, the formulas proposed by Verhoff and Banchero, and Okkes are considered to better match experimental results. However, the Verhoff and Banchero formula still overestimates by 4 °C or more at an acid dew point of 120−140 °C, while the Okkes formula underestimates the acid dew point at low water vapor concentrations.[32] In recent years, Xiang et al.[33] and Bahadori[34] have proposed semiempirical formulas based on experimental data. ZareNezhad and Aminian[35] used neural network algorithms to calculate the acid dew point. These methods provide new insights for calculating the acid dew point, but understanding and calculating the acid dew point from the perspective of condensation process theory still require further exploration.

In coal-fired flue gas, binary condensation of H_2SO_4−H_2O may also occur on particle surfaces with a high curvature. Yan[36] directly observed the phenomenon of particle surface roughening at temperatures below the acid dew point in experiments using SEM. Previous studies[37−40] with field tests found that dust removal equipment exhibits significant synergistic removal effects on SO_3, indicating that some sulfuric acid deposits on particles are removed. Huang[41] and Wu[42] pointed out that in WFGD, due to higher water vapor concentration, sulfuric acid mist is prone to form and be synergistically removed. The wESP device downstream of WFGD is considered the most effective device for sulfuric acid mist removal[9] because the electric force can significantly enhance the aggregation and growth of sulfuric acid mist droplets,[43] thereby enhancing its removal efficiency. The above studies all suggest that gaseous H_2SO_4 can condense and adhere to particles in the flue gas system units. Researchers also conducted numerical simulations to study the binary condensation of H_2SO_4−H_2O on particle surfaces.[44] The adopted condensation models often set a specific value of nucleation rate as the criterion for the initiation of H_2SO_4−H_2O condensation.[45] However, there is currently no agreement on the selection of this value, and different values can lead to significant differences in the condensation initiation conditions and processes. Based on thermodynamic analysis, the large curvature of particle surfaces yields a large saturation vapor pressure of condensable components on sulfuric acid liquid film surfaces, resulting in small acid dew points under the same gas-phase concentration conditions compared to those on the planar surface. Therefore, the formulas of the acid dew point proposed for binary condensation on planar surfaces are not applicable to particle surfaces. Further research is needed on the conditions of binary condensation of H_2SO_4−H_2O on particle surfaces, and corresponding predictive formulas remain to be proposed.

To address the above issues, this study establishes a phase equilibrium model for binary condensation of H_2SO_4−H_2O on both planar and fly ash particle surfaces based on thermodynamic theory and investigates the corresponding phase equilibrium states of H_2SO_4−H_2O binary condensation. From the perspective of thermodynamic analysis, the physical meaning of the planar acid dew point is clarified. Based on this, a more accurate predictive formula over a wide range of gas-phase parameters is proposed, along with a predictive formula for the concentration of equilibrium liquid film sulfuric acid. The phase equilibrium states of acid condensation on particle surfaces of different sizes are studied, and predictive formulas for the phase equilibrium parameters of the binary condensation process of H_2SO_4−H_2O on particle surfaces are established. The results can provide guidance for the

https://doi.org/10.1021/acsomega.5c00382
ACS Omega 2025, 10, 19625−19635

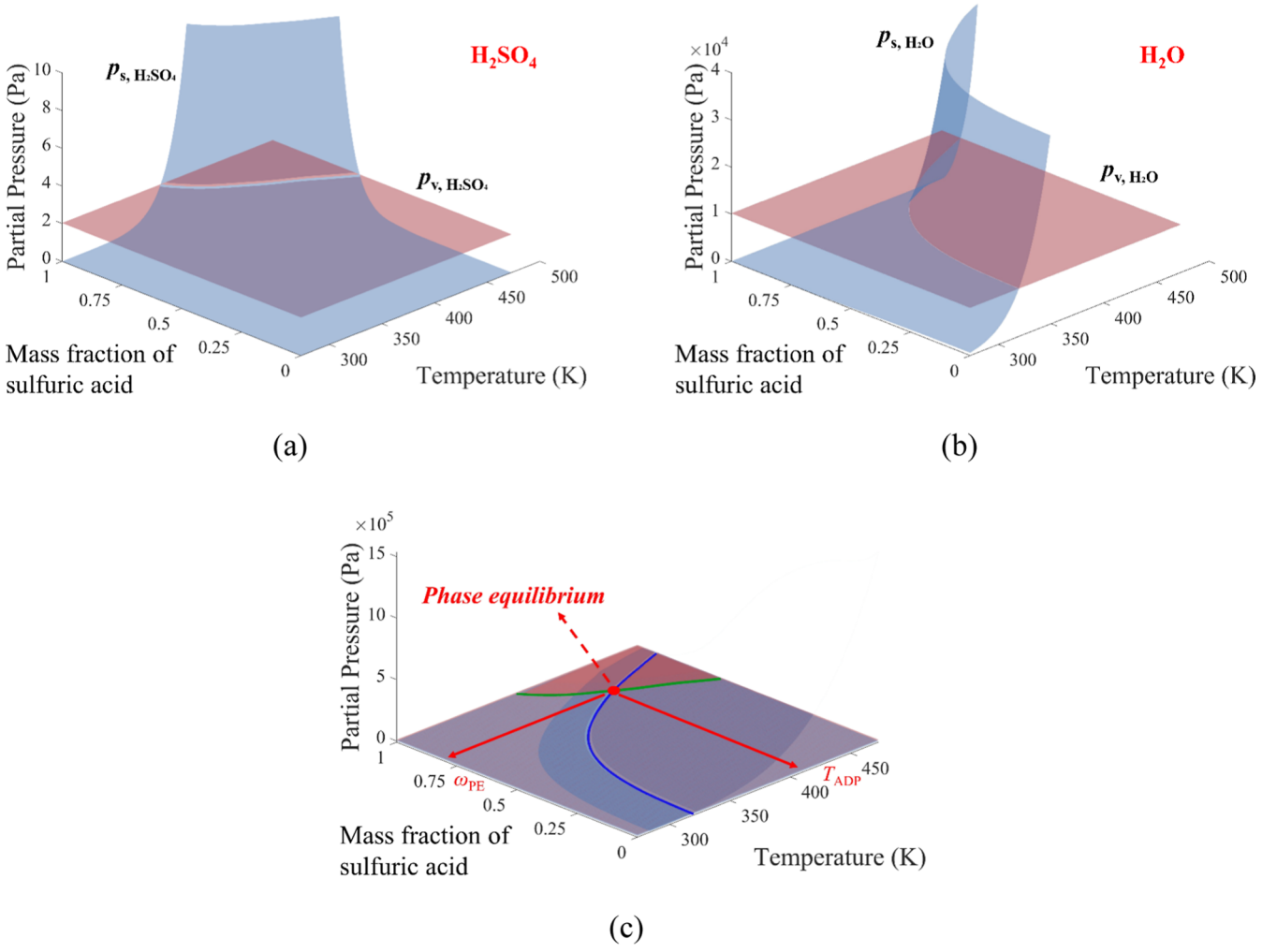

Figure 2. Graphical solution for determining the phase equilibrium of (a) H_2SO_4, (b)H_2O and (c) binary equilibrium point. Here, c_{v,H_2SO_4} = 20 ppm, c_{v,H_2O} = 10%.

prevention of low-temperature corrosion in flue gas and reduction of sulfuric acid mist emissions.

2. MODELS AND NUMERICAL METHODS

2.1. Theoretical Model. This study investigates the phase equilibrium parameters for the binary condensation of H_2SO_4−H_2O on the surfaces of planes and particles with different diameters in flue gas with gas-phase component partial pressures of p_{v,H_2SO_4} and p_{v,H_2O}. At the microscopic level, the fundamental difference between the evaporation and condensation processes lies in the magnitudes of the interfacial mass fluxes I_{v-l} and I_{l-v} across the gas−liquid interface. As illustrated in Figure 1, the conditions for binary condensation of H_2SO_4−H_2O depend on the relationship between the intensive variables of each condensing component when phase equilibrium (equal interfacial mass fluxes, $I_{v-l} = I_{l-v}$) is achieved. Here, we assume that the surfaces of planes and particles are coated by a thin film of sulfuric acid solution, as indicated by the blue region in the figure. The gas phase with a condensable component concentration of $p_{v,i}$ is shown as the yellow region, where i represents different condensable components (H_2O or H_2SO_4). Following Gibbs,[12] we define the red dotted line in the sketches as a gas−liquid dividing surface, on which we have the thermal equilibrium, mechanical equilibrium, and phase equilibrium between the phases, respectively shown in eqs 1−3.

$$T_{v,i} = T_{l,i} = T \tag{1}$$

$$\sum p_{v,i} + \Delta p = \sum p_{l,i} \tag{2}$$

$$\mu_{v,i} = \mu_{l,i} \tag{3}$$

where T, p, and μ represent the temperature, pressure, and chemical potential, and the subscript "v" and "l" represent the vapor and liquid phases. $p_{v,i} = p_{total} \times V_i$, where p_{total} is the total pressure of the environment and V_i is the volume fraction of component i in the gas phase. $\Delta p = 2\sigma/r$, representing the Laplace pressure across the gas−liquid interface, where r is the radius of curvature of the gas−liquid surface, which is assumed to equal to the particle radius here. σ is the surface tension of the sulfuric acid solution, which can be calculated as[46]

$$\sigma = \left(a + b\left(1 - \frac{T}{T_p}\right)\right)\left(1 - \frac{T}{T_p}\right)^{1.256} \tag{4}$$

$$a = 0.2358 - 0.529x + 4.073x^2 - 12.6707x^3 + 15.3552x^4 - 6.3138x^5 \tag{5}$$

https://doi.org/10.1021/acsomega.5c00382
ACS Omega 2025, 10, 19625−19635

$$b = -0.14738 + 0.6253x - 5.4808x^2 + 17.2366x^3 - 21.0487x^4 + 8.719x^5 \quad (6)$$

$$T_p = 647.15(1 - x)^2 + 900.0x^2 + 3156.186x(1 - x) \quad (7)$$

where x is the mole fraction of sulfuric acid in the solution, and T_p is the pseudocritical temperature of the binary solution.

We can derive the binary Kelvin equation through explicit thermodynamic equilibrium analysis. For each component i ($i = H_2O, H_2SO_4$), the chemical potentials in vapor (v) and liquid (l) phases must satisfy chemical potential equality (eq 3); the equality ensures no net mass transfer across the gas−liquid interface ($I_{v-l} = I_{l-v}$).

Assuming the vapor behaves as an ideal gas, the chemical potential of component i in the vapor phase can be expressed as

$$\mu_{i,v} = \mu_i^0(T) + RT\ln(p_{v,i}/p_{i,0}) \quad (8)$$

where $\mu_i^0(T)$ is the standard chemical potential of pure component i at temperature T and reference pressure $p_{i,0}$, defined as the saturation vapor pressure over a flat surface. R is the universal gas constant and $p_{v,i}$ is the partial pressure of component i in the vapor phase.

For the liquid phase, the chemical potential incorporates both the nonideal behavior of the solution and the curvature-induced pressure difference (Laplace pressure). The chemical potential of component i in the liquid film is given as

$$\mu_{i,l} = \mu_i^0(T) + RT\ln \alpha_i + V_{m,i}\Delta p \quad (9)$$

where α is the activity of component in the solution, $V_{m,i}$ is the partial molar volume of component i, which is also affected by the sulfuric acid mass fraction ω of the solution. Based on data from Perry's Chemical Engineers' Handbook,[47] we fitted the following linear regression equation based on mass fraction for calculation purposes

$$V_{m,H_2SO_4} = 53.3 - 20.0 \times \omega \quad (10a)$$

$$V_{m,H_2O} = 18.0 - 10.0 \times \omega \quad (10b)$$

Equating the vapor and liquid chemical potentials (eqs 8 and 9) yields

$$RT\ln(p_{v,i}/p_{i,0}) = RT\ln \alpha_i + V_{m,i}(2\sigma/r) \quad (11)$$

Rearranging eq 11 provides the generalized Kelvin equation for binary condensation

$$p_{v,i} = \alpha_i p_{i,0}\exp\left(\frac{2\sigma V_{m,i}}{rRT}\right) = p_{s,i}\exp\left(\frac{2\sigma V_{m,i}}{rRT}\right) \quad (12)$$

where p_{s,H_2SO_4} and p_{s,H_2O} are the saturated vapor pressure of the condensable component, determined by the sulfuric acid mass fraction ω and the temperature T of the solution. We use the data reported in Perry's Chemical Engineers' Handbook[47] to obtain the value of $p_{s,i}$ via interpolation. Based on the aforementioned data, the solute−solvent interactions reflected by the activity are simplified. The exponential term quantifies the enhancement of the vapor pressure over curved surfaces.

According to the Gibbs phase rule, a binary, two-phase system has 2 independent intensive variables in equilibrium. In this study, the concentrations of gaseous H_2SO_4 and H_2O are known, constituting 2 independent intensive variables, which are sufficient to determine the phase equilibrium state. The temperature (acid dew point, T_{ADP}) and the mass fraction of the solution (equilibrium liquid film sulfuric acid mass fraction, ω_{PE}) at equilibrium can be solved by combining eq 12 and the relationship between $p_{s,i}$ and ω, T obtained from Perry's Chemical Engineers Handbook (with the variables to be solved being: T_{ADP}, ω_{PE}, p_{s,H_2SO_4}, p_{s,H_2O}). The detailed calculation method is described below.

2.2. Numerical Methods. For the binary condensation on a planar surface, eq 12 simplifies to $p_{v,i} = p_{s,i}$. We use the graphical solution in MATLAB 2022a to determine $T_{ADP,plane}$ and $\omega_{PE,plane}$, and the calculation steps are sketched in Figure 2. The blue surface represents the $p_{s,i}$ obtained through two-dimensional cubic spline interpolation based on the data in Perry's Chemical Engineers' Handbook,[47] with solution sulfuric acid mass fraction ω and temperature T as two variables. The red plane represents the vapor component partial pressures ($p_{v,i}$). The sketches for the calculation of sulfuric acid and water components are shown in Figure 2a,b, respectively. When the blue surface intersects with the red plane, the condensable component satisfies $p_{s,i} = p_{v,i}$, and the intersection lines yield the corresponding T and ω through graphical methods. Projecting the two intersection lines in Figure 2a,b onto the $T-\omega$ plane, we obtain the green and blue curves in Figure 2c, respectively. The intersection point indicated by the red point in the figure represents the equilibrium conditions for the binary condensation of H_2SO_4 and H_2O. The acid dew point ($T_{ADP,plane}$) and the equilibrium liquid film sulfuric acid mass fraction ($\omega_{PE,plane}$) on the planar surface are then obtained as the temperature and mass fraction corresponding to the intersection point in Figure 2c.

For particles with a large surface curvature, the Kelvin effect cannot be ignored, and eq 12 is solved iteratively. Given the gas-phase component concentrations ($p_{v,i}$), assume an initial liquid film temperature $T^{(0)} = T_{ADP,plane}$, and mass fraction $\omega^{(0)} = \omega_{PE,plane}$ to start the calculation. Using the iteratively computed liquid film temperature ($T^{(k-1)}$) and mass fraction ($\omega^{(k-1)}$) as inputs (where $k \geq 1$ represents the iteration step), based on eqs 4−7, $p_{s,i}^{(k-1)} = p_{v,i}/\exp\left(\frac{2\sigma^{(k-1)}V_m^{(k-1)}}{rRT^{(k-1)}}\right)$ is solved. It should be noted that σ and V_m both vary with the sulfuric acid mass fraction (ω) inside the liquid film as intermediate variables for the iteration. Then, using the graphical method employed in the previous section, the liquid film temperature and mass fraction corresponding to the saturation vapor pressure combination are determined, yielding $T^{(k)}$ and $\omega^{(k)}$. This process constitutes a single iteration step. Convergence is achieved when $(T^{(k)} - T^{(k-1)})/T^{(k-1)} < 0.001$ and $(\omega^{(k)} - \omega^{(k-1)})/\omega^{(k-1)} < 0.001$. The corresponding liquid film temperature $T^{(k)}$ and mass fraction $\omega^{(k)}$ are then considered as the particle acid dew point ($T_{ADP,particle}$) and equilibrium liquid film sulfuric acid mass fraction ($\omega_{PE,particle}$) on the surface of a particle of diameter d_p at gas-phase component concentration $p_{v,i}$.

In the calculation of the binary condensation of H_2SO_4−H_2O on the plane, the H_2SO_4 vapor concentration ranges from 0.5 to 50 ppm and the H_2O vapor concentration ranges from 0.5% to 15%, covering 3000 operating conditions. For the calculation of the binary condensation of H_2SO_4−H_2O on particle surfaces, the main operating conditions selected are shown in Table 1, with particle diameters ranging from 1 nm to 100 μm.

https://doi.org/10.1021/acsomega.5c00382
ACS Omega 2025, 10, 19625−19635

Table 1. Parameters for Numerical Calculations of Binary Condensation of H_2SO_4–H_2O on Particle Surfaces

parameters	values
diameter of particle, $d_p = 2r$ (μm)	100, 10, 1, 0.1, 0.01, 0.001
volume fraction of H_2SO_4 in vapor, c_{v,H_2SO_4} (ppm)	1, 2.5, 5, 7.5, 10, 15, 20, 25, 30, 40, 50
volume fraction of H_2O in vapor, c_{v,H_2O} (%)	2, 5, 7, 10, 13, 15

3. RESULTS AND DISCUSSION

3.1. Equilibrium State of Sulfuric Acid Binary Condensation at Planar Surfaces. As a start, this section focuses on the conditions for binary condensation of H_2SO_4–H_2O on a plane, and the reliability of the calculation method in this study is validated through a comparison of the calculated results to previously reported data. Figure 3a presents the isothermal diagram of $T_{ADP,plane}$ of the binary condensation under different concentrations of H_2SO_4 and H_2O. It can be observed that as the concentrations of H_2SO_4 and H_2O increase, $T_{ADP,plane}$ increases, with a slower increasing rate at a higher component concentration. Table 2 shows the $T_{ADP,plane}$ corresponding to an H_2O volume fraction of 8%–10% and an H_2SO_4 volume fraction of 0.5/5/10/15/20/30/40/50 ppm.

Figure 3b presents the $\omega_{PE,plane}$ under different concentrations of H_2SO_4 and H_2O in the vapor phase. The $\omega_{PE,plane}$ increases with an increasing H_2SO_4 vapor concentration and a decreasing H_2O vapor concentration. Within the range of condensable component concentrations ($V_{H_2SO_4}$ = 0.5 ppm-50 ppm, V_{H_2O} = 0.5%–15%) in this study, the sulfuric acid mass fraction in the planar liquid film ranges from 71.922% to 91.058%. Zuo et al.[24] found that the corrosion rate decreases when the mass fraction of sulfuric acid solution exceeds 60%. Moreover, the strong oxidation of concentrated sulfuric acid forms metal oxides on the metal surface, creating a protective layer that further mitigates corrosion. Therefore, the sulfuric acid solution film formed near the acid dew point exhibits low corrosivity to equipment due to its high concentration. This partially explains why significant corrosion of heat exchange surfaces typically occurs only at temperatures several degrees below the acid dew point reported by previous studies.[48]

Figure 4 compares the $T_{ADP,plane}$ calculated in this study with the experimental results of ZareNezhad[49] and Blanco[32] under the same H_2SO_4 and H_2O vapor concentrations. In the plot, under identical operating conditions, the x-axis of the data points represents the results calculated by the model proposed in this study, while the y-axis corresponds to the data from previously reported experiments or models. The red dashed line indicates the line of perfect agreement between the two data sets. The data points we calculated have an average deviation of +1.27 °C and a maximum deviation of +5.18 °C compared to ZareNezhad's experiments and an average deviation of −2.67 °C and a maximum deviation of −4.62 °C compared to Blanco's results. This indicates that $T_{ADP,plane}$ obtained using the thermodynamic phase equilibrium-based calculation method we adopted is in good agreement with the reported experimental data. Taking the $T_{ADP,plane}$ calculated in this study as a reference, several sets of empirical formulas that consider the influence of both H_2SO_4 and H_2O vapor concentrations on the $T_{ADP,plane}$ are evaluated, also as shown in Figure 4. The calculation results of the Bapahoba formula are generally lower compared with the numerical results in this study, while the Verhoff formula yields higher values compared with the numerical calculation results in this study. The formula from the Japan Institute of Electric Power Industry for a 10% H_2O vapor concentration matches our numerical results the best, with average deviations of −2.16 °C and +2.70 °C for H_2O vapor concentrations of 5% and 15%, respectively. The Okkes formula exhibits the best agreement with our numerical results at H_2O vapor concentrations above 10%. However, as indicated by the data within the blue dot-lined box in Figure 4, at low H_2O vapor concentrations, the $T_{ADP,plane}$ calculated by this formula is lower than the numerical results in this study, consistent with a previous report that the Okkes formula exhibits lower accuracy at low H_2O vapor concentrations.[32]

In the condensation process, the thermodynamic equilibrium state calculated in this study corresponds to the critical state, where the sulfuric acid–water binary mixture formed can be regarded as a thin liquid film but that has not yet undergone significant condensation (otherwise, $p_{v,i} > p_{s,i}$). Therefore, the planar acid dew point defined in this study represents the highest upper temperature limit at which macroscopic condensation is thermodynamically permissible. In actual experimental observations of the planar acid dew point temperature, the measurement by the dew point meter requires the accumulation of a certain thickness of the sulfuric

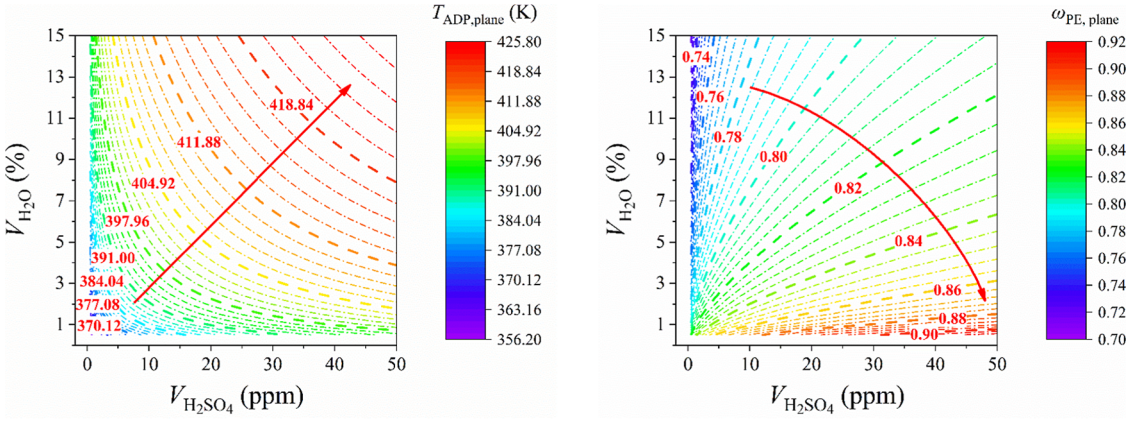

Figure 3. Equilibrium parameters for the binary condensation of H_2SO_4–H_2O on the planar surface: (a) $T_{ADP,plane}$ and (b) $\omega_{PE,plane}$.

https://doi.org/10.1021/acsomega.5c00382
ACS Omega 2025, 10, 19625–19635

Table 2. Acid Dew Points ($T_{ADP,Plane}$ (K)) at Different Concentrations of H_2SO_4 with 8%−10% H_2O

$V_{H_2SO_4}$, V_{H_2O}	0.5 ppm	5 ppm	10 ppm	15 ppm	20 ppm	30 ppm	40 ppm	50 ppm
8%	383.4	398.5	403.99	407.49	410.1	413.94	416.75	418.99
8.5%	384.17	399.19	404.65	408.13	410.73	414.56	417.37	419.61
9%	384.89	399.86	405.28	408.73	411.33	415.15	417.96	420.2
9.5%	385.58	400.5	405.88	409.31	411.89	415.71	418.52	420.76
10%	386.24	401.11	406.46	409.87	412.44	416.25	419.05	421.29

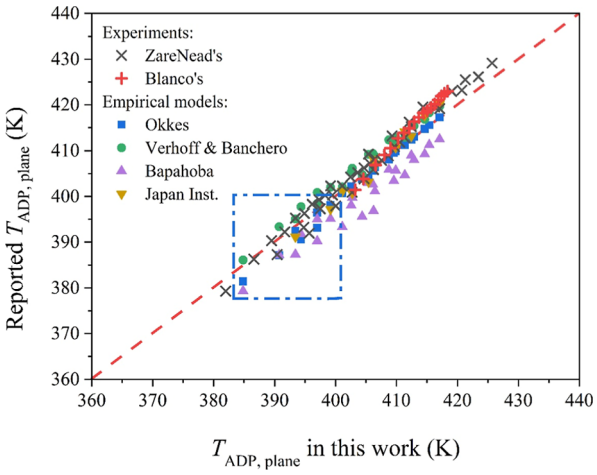

Figure 4. Comparison between $T_{ADP,plane}$ calculated by this study and the experimental results as well as the predicted results from empirical formulas in the literature.

acid liquid film, resulting in significant variations in electrical signals. The temperature recorded under such conditions should therefore be lower than the onset temperature of acid condensation, that is, the planar acid dew point temperature $T_{ADP,planar}$ defined in this study. Variations in measurement methodologies, condensation criteria, and instrument precision adopted by different researchers inevitably lead to discrepancies in the experimentally measured acid dew points. Employing electrical signal measurement devices with higher sensitivity and stricter critical electrical signal thresholds can yield results that more closely approximate the thermodynamic equilibrium state of sulfuric acid condensation.

3.2. Equilibrium State of Sulfuric Acid Condensation on the Particle Surface. Regarding the condensation of sulfuric acid on fly ash particles in flue gas, the large curvature of particle surfaces prevents them from being approximated as flat surfaces. We study the conditions of sulfuric acid condensation on particle surfaces in this section, where the particle is approximated as spherical. Figure 5 presents the acid dew point ($T_{ADP,particle}$) on the surfaces of particles of different diameters. The $T_{ADP,particle}$ on particle surfaces increases rapidly with the condensable component concentration, and the growth rate gradually slows down. This trend is similar to that observed in $T_{ADP,plane}$ on flat surfaces in Figure 3a. However, it can be observed that the $T_{ADP,particle}$ curves for d_p = 1 μm, 10 μm and $T_{ADP,plane}$ curve overlap with each other. The $T_{ADP,particle}$ decreases with particle diameter for submicron particles. This indicates that when the particle diameter is relatively large, the influence of particle surface curvature can be neglected, and the conditions for binary condensation are similar to those on flat surfaces. Only when the particle diameter is smaller than approximately 1 μm, the Kelvin effect needs to be considered to account for the effect of particle curvature.

Figure 6a illustrates the variation of $T_{ADP,particle}$ on particle surfaces with d_p at different H_2SO_4 and H_2O vapor concentrations. It can be observed that particle size significantly influences the $T_{ADP,particle}$, especially in the submicron range. Taking the case with an H_2SO_4 vapor concentration of 20 ppm and an H_2O vapor concentration of 10% as an example, the $T_{ADP,particle}$ for a 0.01 μm particle is 407.41 K, which is 5 K lower than that for a 1 μm particle (412.40 K). This can be explained by eq 12. As the particle diameter decreases, the Kelvin effect causes a decreasing $p_{s,i}$ as well as a decreasing $T_{ADP,particle}$. Further analysis of the exponent shows that the temperature and the mass fraction of sulfuric acid in the equilibrium liquid film vary within a small range of 360 to 430 K and 70% to 90% under different environmental component concentrations in practice, respectively (see Figure 3). On the other hand, the surface tension of the solution (σ), controlled by the solution temperature and mass fraction, does not undergo significant changes (eqs 4−7), while the particle diameter (d_p) can undergo significant changes over several orders of magnitude, greatly influencing the binary condensation conditions. For small particles, the value of the exponent is >1 and decreases with increasing particle size, leading to an increasing $p_{s,i}$. The solution equilibrium parameters on small particle surfaces cannot be simplified, as we showed in Section 3.1, and the corresponding formulas for predicting the $T_{ADP,particle}$ need to be developed. When the particle diameter is relatively large, the value of the exponent approaches 1, and the binary condensation process is similar to that on a flat surface. The differences in the $T_{ADP,particle}$ among particles of different diameters will significantly affect the heterogeneous condensation characteristics of dispersed particles in the flue gas system. Due to the significantly lower $T_{ADP,particle}$ of submicron particles compared to micron-sized particles under the same environmental component concentration conditions, condensation will preferably occur on the surfaces of larger particles, which consumes the condensable gases in the environment and further reduces the $T_{ADP,particle}$ of submicron particles. Therefore, in flue gas systems employing dust collectors for the synergistic removal of SO_3, more attention should be placed on the removal of larger particles, reinforcing the use of dust removal devices based on principles such as inertia separation.[50]

Figure 6b illustrates the variation of the mass fraction of sulfuric acid in the equilibrium liquid film ($\omega_{PE,particle}$) on particle surfaces with different d_p values at various concentrations of gaseous condensable components. It can be observed that in the submicron range, $\omega_{PE,particle}$ decreases significantly with increasing d_p, while in the micron range, $\omega_{PE,particle}$ tends to plateau, barely affected by d_p. $\omega_{PE,particle}$ increases with increasing H_2SO_4 vapor concentration and decreasing H_2O vapor concentration in the gas phase, a trend

https://doi.org/10.1021/acsomega.5c00382
ACS Omega 2025, 10, 19625−19635

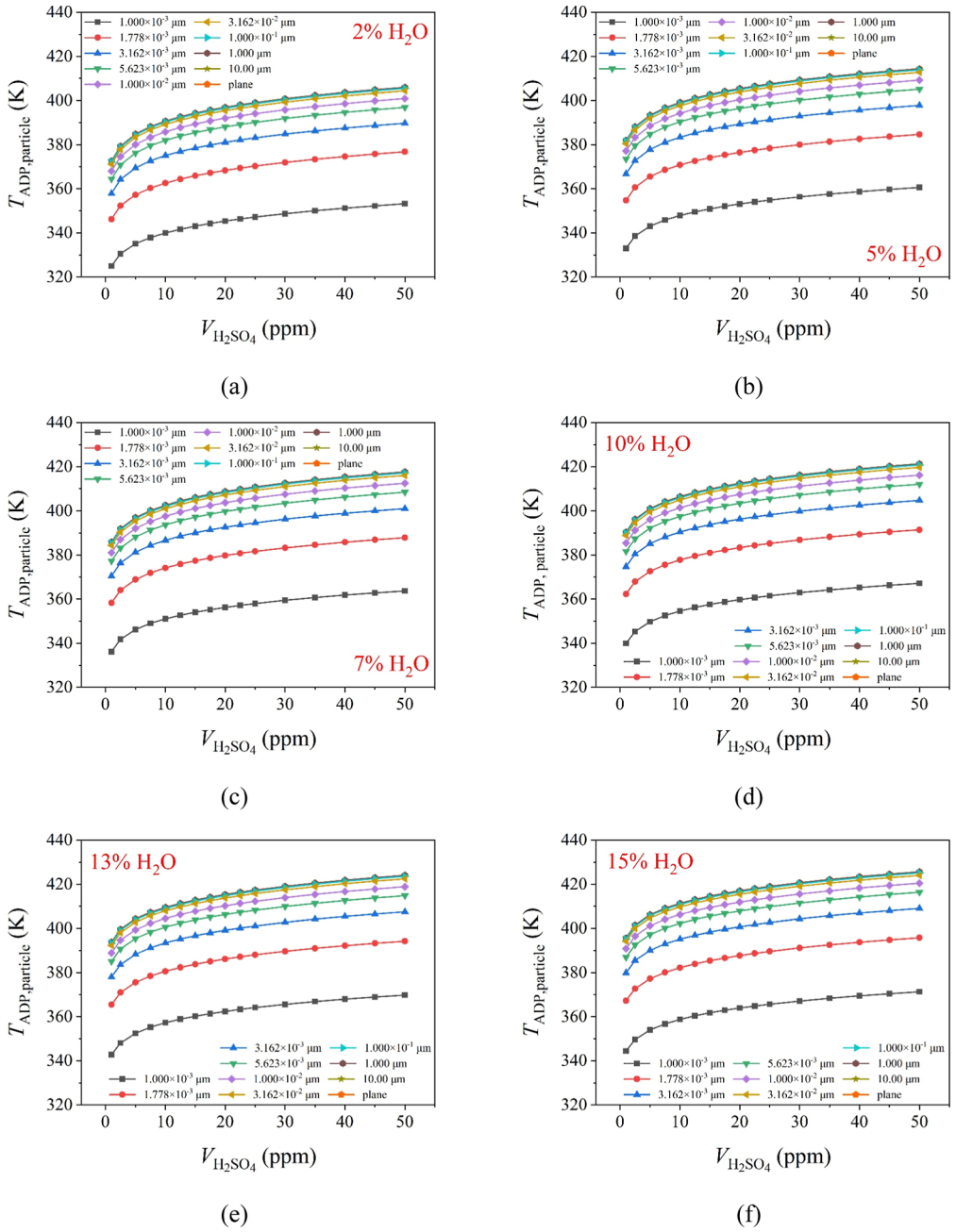

Figure 5. Variation of $T_{ADP,particle}$ with H_2SO_4 concentration in the vapor phase when V_{H_2O} = (a) 2%, (b) 5%, (c) 7%, (d) 10%, (e) 13%, and (f) 15%.

similar to that observed in the variation of $\omega_{PE,plane}$ on flat surfaces, as shown in Figure 3b. In the range of 1−50 ppm of H_2SO_4 vapor concentration and 2−15%H_2O vapor concentration, $\omega_{PE,particle}$ ranges from 73.26% to 89.03%.

3.3. Prediction Formulas for the Equilibrium State of Sulfuric Acid Condensation. The calculation method in Section 2.2 based on thermodynamic theory requires iterations for $T_{ADP,plane}$ and $\omega_{PE,plane}$, which is inconvenient for engineering applications. While several prediction formulas for the $T_{ADP,plane}$ have been proposed for the binary condensation on the planar surface, they all exhibit larger deviations compared to the numerically calculated results in this study. Additionally, there is a lack of prediction methods for the $\omega_{PE,plane}$. Therefore, this section first proposes a new prediction formula with high precision for the $T_{ADP,plane}$ in this study and establishes a prediction formula for the $\omega_{PE,plane}$ based on our numerical results under various gas-phase component concentrations on the planar surface. Based on this, prediction formulas for $T_{ADP,particle}$ and $\omega_{PE,particle}$ on particle surfaces are further proposed.

As indicated in Section 3.1, among the existing $T_{ADP,plane}$ prediction formulas, the Okkes formula[29] exhibits the highest agreement with the numerical calculated $T_{ADP,plane}$ in this study. However, it tends to underestimate the $T_{ADP,plane}$ at low H_2O vapor concentrations (<10%). Therefore, we calculated the $T_{ADP,plane}$ under 1%−9%H_2O, using gas-phase condensable component concentration $p_{v,i}$ as variables. Using the same formula form as Okkes,[29] we refitted the fitting parameters using our data. The coefficients and obtained new formula are shown as eq 13a. For $T_{ADP,plane}$ at H_2O vapor concentrations

https://doi.org/10.1021/acsomega.5c00382
ACS Omega 2025, 10, 19625−19635

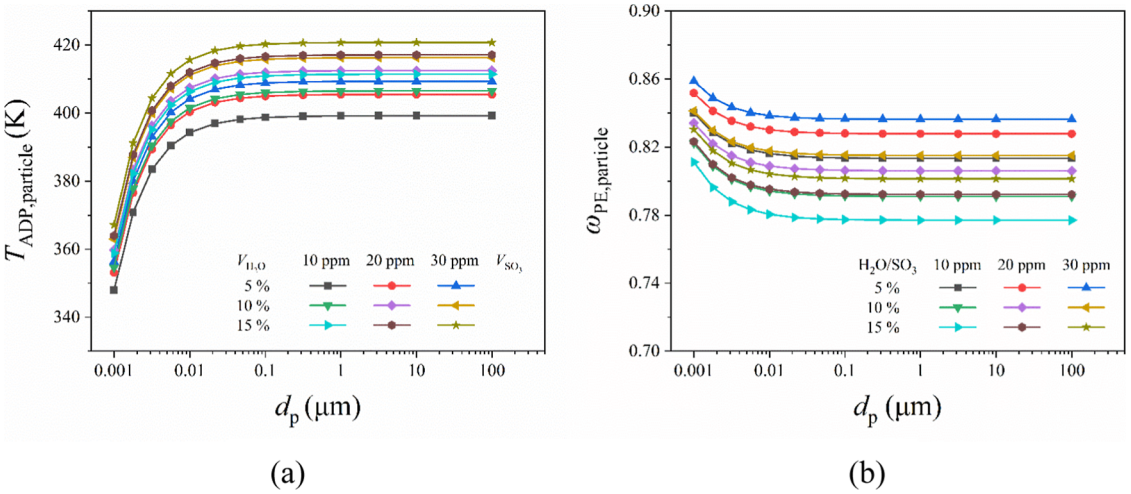

Figure 6. Variation of (a) $T_{ADP,particle}$ and (b) $\omega_{PE,particle}$ with d_p at different concentrations of condensable components.

greater than 10%, the Okkes formula is still employed (Equation 13b).

$$T_{ADP,plane}(°C) = 11.07 + 20.72\lg p_{v,H_2O} - 0.2865\lg p_{v,H_2SO_4} + 2.631 \times (\lg p_{v,H_2SO_4} + 3.82)^2 \quad (V_{H_2SO_4} < 10\%) \tag{13a}$$

$$T_{ADP,plane}(°C) = 10.8809 + 27.6\lg p_{v,H_2O} + 10.83\lg p_{v,H_2SO_4} + 1.06 \times (\lg p_{v,H_2SO_4} + 2.9943)^{2.19} \quad (V_{H_2SO_4} > 10\%) \tag{13b}$$

Equation 13a shows a coefficient of determination of R^2 = 0.9975, well describing our numerical results. In eqs 13a and 13b, the unit of the $T_{ADP,plane}$ is °C, and the independent variable, the concentration of condensable components in the environment ($p_{v,i}$) is in units of Pa.

Considering that $\omega_{PE,plane}$ changes rapidly at first and then slowly with the concentration of condensable components in the gas, a logarithmic function was employed for fitting. The fitted formula is presented in eq 14, with a coefficient of determination of R^2 = 0.9989.

$$\omega_{PE,plane} = 1.073 - 0.07037\lg p_{v,H_2O} + 0.04698\lg p_{v,H_2SO_4} \tag{14}$$

To the best of our knowledge, there are no prediction formulas for the $T_{ADP,particle}$ and the $\omega_{PE,particle}$ on the particle surface with high curvature. Considering that $T_{ADP,particle}$ and $\omega_{PE,particle}$ of large particles tend to approach those of the plane, we use $T_{ADP,plane}$, and $\omega_{PE,plane}$ as reference values. We derive the particle size-dependent coefficients η_T and η_ω for $T_{ADP,particle}$ and $\omega_{PE,particle}$, respectively, as shown in eqs 15a and 15b

$$\eta_T(d_p) = \frac{T_{ADP,particle}(d_p)}{T_{ADP,plane}} \tag{15a}$$

$$\eta_\omega(d_p) = \frac{\omega_{PE,particle}(d_p)}{\omega_{PE,plane}}. \tag{15b}$$

We calculated the average values of η_T and η_ω of the particles with the same diameter at different gas component concentrations, as shown in Figure 7. It can be observed that

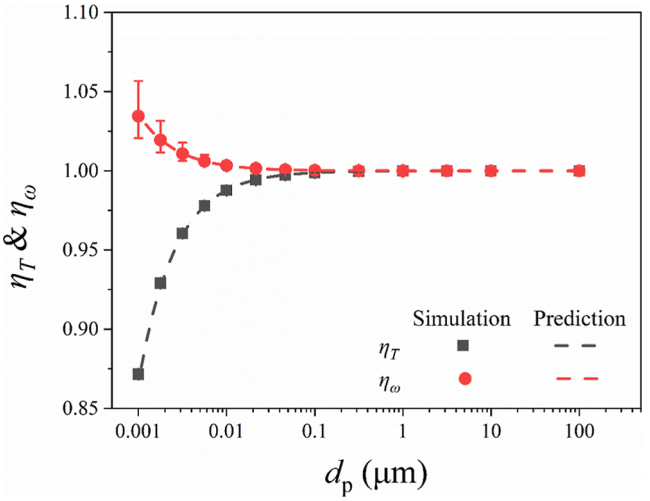

Figure 7. Variations of the particle size-dependent coefficients η_T and η_ω with d_p.

η_T is less than 1 and gradually increases with particle size, tending to approach 1 in the micron range. On the other hand, η_ω is greater than 1 and decreases with increasing particle size, gradually approaching 1 in the micron range. In Figure 7, the upper and lower limits of each data point represent the maximum and minimum values at different gas component concentrations. As the particle diameter decreases, the difference between the maximum and minimum values gradually increases. Nevertheless, the maximum relative deviations of η_T and η_ω (for d_p = 0.001 μm) are only 0.18% and 2.13%, respectively. Therefore, we can conclude that η_T and η_ω are not significantly affected by the component concentration but are mainly dependent on the particle diameter (d_p). Based on this, we can then establish prediction formulas for the equilibrium parameters of binary condensation on particle surfaces.

Fitting the data points in Figure 7, we obtain equations for η_T and η_ω, as shown in eqs 16a and 16b.

https://doi.org/10.1021/acsomega.5c00382
ACS Omega 2025, 10, 19625−19635

$$\eta_T(d_p) = 1 - \frac{d_p^{-1.038}}{9749.78} \quad (16a)$$

$$\eta_\omega(d_p) = 1 + \frac{d_p^{-1.021}}{32500.15} \quad (16b)$$

where d_p is in units of μm, and the correlation coefficients R^2 for eqs 16a and 16b are 0.9994 and 0.9997, respectively. It proves that eqs 16a and 16b well describe our numerical results as shown in Figure 7.

By combining eqs 13a−16b, one can determine $T_{ADP,particle}$ and $\omega_{PE,particle}$ for the H_2SO_4−H_2O binary condensation on particle surfaces at different gas-phase condensable component concentrations.

4. CONCLUSION

This study investigates the SO_3 condensation process in flue gas based on thermodynamic equilibrium theory, with a focus on the heterogeneous condensation of SO_3 with H_2O on both planar and particle surfaces. The numerical model is validated by comparing the obtained acid dew points with previous experimental results, and the influences of the condensable component concentration and particle diameter on the acid dew point and equilibrium sulfuric acid mass fraction are analyzed.

On the planar surface, the acid dew point ($T_{ADP,plane}$) increases rapidly at first and then more slowly as the gas concentration increases, while the equilibrium sulfuric acid mass fraction ($\omega_{PE,plane}$) increases with H_2SO_4 concentration and decreases with H_2O concentration. For H_2SO_4 concentrations of 0.5−50 ppm and H_2O concentrations of 0.5%−15%, $T_{ADP,plane}$ ranges from 356.37 to 426.67 K, and $\omega_{PE,plane}$ ranges from 71.922% to 91.058%. Based on the numerical results, a higher-precision predictive formula for $T_{ADP,plane}$ is proposed, and a prediction formula for $\omega_{PE,plane}$ considering the influence of gas-phase binary condensable component concentration is also established.

In the sulfuric acid−water binary condensation on particle surfaces, it is found that the acid dew point ($T_{ADP,particle}$) and the equilibrium sulfuric acid mass fraction ($\omega_{PE,particle}$) of micrometer-sized particles are similar to those of planar surfaces, while those of submicrometer particles are significantly influenced by particle size. As the particle diameter decreases, the Kelvin effect becomes more pronounced, leading to a decrease in $T_{ADP,particle}$ and an increase in $\omega_{PE,particle}$. The ratio of the condensation parameters on particle surfaces to those on planar surfaces is primarily dependent on particle size, and corresponding fitting formulas are derived based on the numerical results. We further propose the prediction formulas for $T_{ADP,particle}$ and $\omega_{PE,particle}$ for particles of different sizes under various gas-phase condensable component concentrations.

The predictive formulas for acid dew point and sulfuric acid mass fraction proposed in this study can provide theoretical support for predicting SO_3 condensation conditions in coal-fired plants, assisting in the development of strategies for low-temperature corrosion prevention and sulfuric acid mist reduction, thereby promoting the advancement of flue gas treatment technologies.

ASSOCIATED CONTENT

Data Availability Statement

This study constitutes a computational analysis and does not involve experimental data sets. All mathematical model derivations and computational parameters have been comprehensively detailed in the manuscript.

Supporting Information

The Supporting Information is available free of charge at https://pubs.acs.org/doi/10.1021/acsomega.5c00382.

MATLAB computational scripts for: planar surface acid dew point (T_{ADP}) calculations and curved particle surface equilibrium concentration solver (Kelvin effect correction), and thermodynamic databases: H_2SO_4−H_2O vapor−liquid equilibrium(VLE) data (PDF)

AUTHOR INFORMATION

Corresponding Authors

Bingqiang Ji − *School of Astronautics, Beihang University, 100191 Beijing, China*; Email: bingqiangji@buaa.edu.cn

Qiang Song − *Department of Energy and Power Engineering, Tsinghua University, Beijing 100084, China*; orcid.org/0000-0002-5484-3594; Phone: +86 10 62781740; Email: qsong@tsinghua.edu.cn; Fax: +86 10 62781740

Authors

Zuozhou Tang − *Department of Energy and Power Engineering, Tsinghua University, Beijing 100084, China*

Zhongwei Li − *Department of Energy and Power Engineering, Tsinghua University, Beijing 100084, China*

Complete contact information is available at: https://pubs.acs.org/10.1021/acsomega.5c00382

Notes

The authors declare no competing financial interest.

ACKNOWLEDGMENTS

This work was financially supported by the China National Key Research and Development Program (2022YFC3701503), the China National Key Research and Development Program (2022YFB4100201), and the Fundamental Research Funds for the Central Universities of China (2022ZFJH04). This work was supported by Center of High Performance Computing, Tsinghua University.

NOMENCLATURE

Symbol

c_v	volume fraction
d_p	particle diameter, μm
I	interfacial mass flux, kg·m^{-2}·s^{-1}
p	pressure, Pa
R	universal gas constant, J·mol^{-1}·K^{-1}
r	radius of curvature of gas−liquid interface, m
T	temperature, K
V_m	partial molar volume, m^3·mol^{-1}
α	activity
μ	chemical potential, J·mol^{-1}
σ	surface tension, N·m^{-1}
ω	sulfuric acid mass fraction
η	particle size correction factor

Subscripts

ADP	acid dew point

H_2O	water
H_2SO_4	sulfuric acid
i	component identifier (H_2SO_4 or H_2O)
l	liquid phase
PE	phase equilibrium
plane	planar surface
particle	particle surface
s	saturation state
v	vapor phase.

REFERENCES

(1) Belo, L. P.; Elliott, L. K.; Stanger, R. J.; Spörl, R.; Shah, K. V.; Maier, J.; Wall, T. F. High-Temperature Conversion of SO_2 to SO_3: Homogeneous Experiments and Catalytic Effect of Fly Ash from Air and Oxy-fuel Firing. *Energy Fuels* **2014**, *28* (11), 7243−7251.

(2) Zheng, C. H.; Wang, Y. F.; Liu, Y.; Yang, Z. D.; Qu, R. Y.; Ye, D.; Liang, C. S.; Liu, S. J.; Gao, X. Formation, transformation, measurement, and control of SO_3 in coal-fired power plants. *Fuel* **2019**, *241*, 327−346.

(3) Lu, J.; Zhou, Z.; Zhang, H.; Yang, Z. Influenced factors study and evaluation for SO_2/SO_3 conversion rate in SCR process. *Fuel* **2019**, *245*, 528−533.

(4) Li, Y.; Xiong, J.; Lin, Y.; Guo, J.; Zhu, T. Distribution of SO_2 Oxidation Products in the SCR of NO over V_2O_5/TiO_2 Catalysts at Different Temperatures. *Ind. Eng. Chem. Res.* **2020**, *59* (11), 5177−5185.

(5) Xiong, J.; Li, Y.; Lin, Y.; Zhu, T. Formation of sulfur trioxide during the SCR of NO with NH_3 over a V_2O_5/TiO_2 catalyst. *RSC Adv.* **2019**, *9* (67), 38952−38961.

(6) Forzatti, P. Present status and perspectives in de-NO_x SCR catalysis. *Appl. Catal., A* **2001**, *222* (1−2), 221−236.

(7) Cao, Y.; Zhou, H. C.; Jiang, W.; Chen, C. W.; Pan, W. P. Studies of the Fate of Sulfur Trioxide in Coal-Fired Utility Boilers Based on Modified Selected Condensation Methods. *Environ. Sci. Technol.* **2010**, *44* (9), 3429−3434.

(8) Zhang, Y.; Zheng, C. H.; Liu, S. J.; Qu, R. Y.; Yang, Y. L.; Zhao, H. T.; Yang, Z. D.; Zhu, Y.; Gao, X. An Investigation of SO_3 Control Routes in Ultra-low Emission Coal-fired Power Plants. *Aerosol Air Qual. Res.* **2019**, *9* (12), 2908−2916.

(9) Wang, Y. F.; Gao, W. C.; Zhang, X. F.; Zhang, H.; Liu, W. J.; Chen, Y. J.; Shao, L. Y.; Wu, Z. C.; Dai, H. B.; Zheng, C. H.; et al. Exploring the role of sulfuric acid aerosol in corona discharge through a honeycomb wet electrostatic precipitator. *Process Saf. Environ. Prot.* **2021**, *146*, 763−769.

(10) Reiner, T.; Arnold, F. Laboratory flow reactor measurements of the reaction SO_3+H_2O+m- H_2SO_4+m - implications for gaseous H_2SO_4 and aerosol formation in the plumes of jet aircraft. *Geophys. Res. Lett.* **1993**, *20* (23), 2659−2662.

(11) Vainio, E.; Fleig, D.; Brink, A.; Andersson, K.; Johnsson, F.; Hupa, M. Experimental Evaluation and Field Application of a Salt Method for SO_3 Measurement in Flue Gases. *Energy Fuels* **2013**, *27* (5), 2767−2775.

(12) Kalikmanov, V. I. *Nucleation Theory*; Springer, 2013; .

(13) Carey, V. P. *Liquid-vapor phase-change phenomena: an introduction to the thermophysics of vaporization and condensation processes in heat transfer equipment*; CRC Press, 2020; .

(14) Brachert, L.; Mertens, J.; Khakharia, P.; Schaber, K. The challenge of measuring sulfuric acid aerosols: Number concentration and size evaluation using a condensation particle counter (CPC) and an electrical low pressure impactor (ELPI+). *J. Aerosol Sci.* **2014**, *67*, 21−27.

(15) Yang, Z. D.; Zheng, C. H.; Zhang, X. F.; Zhou, H.; Silva, A. A.; Liu, C. Y.; Snyder, B.; Wang, Y.; Gao, X. Challenge of SO_3 removal by wet electrostatic precipitator under simulated flue gas with high SO_3 concentration. *Fuel* **2018**, *217*, 597−604.

(16) Huijbregts, W. M. M.; Leferink, R. G. I. Latest advances in the understanding of acid dewpoint corrosion: corrosion and stress corrosion cracking in combustion gas condensates. *Anti-Corros. Methods Mater.* **2004**, *51* (3), 173−188.

(17) Pei, T.; Ma, S.; Zhao, G.; Zhao, M. Experimental and numerical studies on capture of SO_3 aerosols from flue gas using finned tube condenser with vortex generators. *Chem. Eng. Process.* **2024**, *195*, 109637.

(18) Wei, W.; Sun, F.; Ma, L. Effect of fine ash particles on formation mechanism of fouling covering heat exchangers in coal-fired power plants. *Appl. Therm. Eng.* **2018**, *142*, 269−277.

(19) Wang, Y.-G.; Zhao, Q.-X.; Zhang, Z.-X.; Zhang, Z.-C.; Tao, W.-Q. Mechanism research on coupling effect between dew point corrosion and ash deposition. *Appl. Therm. Eng.* **2013**, *54* (1), 102−110.

(20) Shen, J. L.; Zheng, C. H.; Xu, L. J.; Zhang, Y.; Zhang, Y. X.; Liu, S. J.; Gao, X. Atmospheric emission inventory of SO_3 from coal-fired power plants in China in the period 2009−2014. *Atmos. Environ.* **2019**, *197*, 14−21.

(21) Srivastava, R. K.; Miller, C. A.; Erickson, C.; Jambhekar, R. Emissions of sulfur trioxide from coal-fired power plants. *J. Air Waste Manage. Assoc.* **2004**, *54* (6), 750−762.

(22) Ebara, R.; Tanaka, F.; Kawasaki, M. Sulfuric acid dew point corrosion in waste heat boiler tube for copper smelting furnace. *Eng. Failure Anal.* **2013**, *33*, 29−36.

(23) Lee, B. H.; Jo, M. H.; Yoo, Y. H. The Effect of Flue Gas Environment on the Corrosion Behavior of the Sulfuric Acid Dew-Point Corrosion Resistant Steel. *Mater. Sci. Forum* **2018**, *941*, 1705−1709.

(24) Zuo, W.; Zhang, X.; Li, Y. Review of flue gas acid dew-point and related low temperature corrosion. *J. Energy Inst.* **2020**, *93* (4), 1666−1677.

(25) Müller, P. Beitrag zur Frage des Einflusses der Schwefelsäure auf die Rauchgas-Taupunkttemperatur. *Chem. Ing. Tech.* **1959**, *31* (5), 345−351.

(26) Abel, E. The vapor phase above the system sulfuric acid-water. *J. Phys. Chem.* **1946**, *50* (3), 260−283.

(27) Halstead, W. D.; Talbot, J. R. W. The sulfuric-acid dewpoint in power-station flue-gases. *J. Inst. Energy* **1980**, *53* (416), 142−145.

(28) Banchero, J. T.; Verhoff, F. H. Evaluation and interpretation of vapor-pressure data for sulfuric-acid aqueous-solutions with application to flue gas dewpoints. *J. Inst. Fuel* **1975**, *48* (395), 76−80.

(29) Okkes, A. G. Get acid dew-point of flue-gas. *Hydrocarbon Process.* **1987**, *66* (7), 53−55.

(30) Puck, T. T. An automatic dewpoint meter for the determination of condensable vapors. *Rev. Sci. Instrum.* **1948**, *19* (1), 16−23.

(31) Stuart, D. D. Acid dewpoint temperature measurement and its use in estimating sulfur trioxide concentration. *ISA Automation Week* **2010**, *2010*, 340−351.

(32) Blanco, J. M.; Peña, F. Increase in the boiler's performance in terms of the acid dew point temperature: Environmental advantages of replacing fuels. *Appl. Therm. Eng.* **2008**, *28* (7), 777−784.

(33) Xiang, B.; Zhang, M.; Yang, H.; Lu, J. Prediction of Acid Dew Point in Flue Gas of Boilers Burning Fossil Fuels. *Energy Fuels* **2016**, *30* (4), 3365−3373.

(34) Bahadori, A. Estimation of combustion flue gas acid dew point during heat recovery and efficiency gain. *Appl. Therm. Eng.* **2011**, *31* (8−9), 1457−1462.

(35) ZareNezhad, B.; Aminian, A. A multi-layer feed forward neural network model for accurate prediction of flue gas sulfuric acid dew points in process industries. *Appl. Therm. Eng.* **2010**, *30* (6−7), 692−696.

(36) Yan, Y.; Sun, K.; Sun, Y.; Zhang, Y.; Guo, J.; Deng, L.; Che, D. Adsorption and Agglomeration Characteristics of Ash Particles after Reducing Flue Gas Temperature below the Acid Dew Point. *9th International Conference on Applied Energy (ICAE)*, 2017, *142*, 3301−3306..

(37) Xu, Y. S.; Liu, X. W.; Cui, J.; Chen, D.; Xu, M. H.; Pan, S. W.; Zhang, K.; Gao, X. P. Field Measurements on the Emission and Removal of $PM_{2.5}$ from Coal-Fired Power Stations: 4. PM Removal

https://doi.org/10.1021/acsomega.5c00382
ACS Omega 2025, 10, 19625−19635

Performance of Wet Electrostatic Precipitators. *Energy Fuels* **2016**, *30* (9), 7465−7473.
(38) Liang, Y. G.; Li, Q.; Ding, X.; Wu, D.; Wang, F. Y.; Otsuki, T.; Cheng, Y.; Shen, T. X.; Li, S. Y.; Chen, J. M. Forward ultra-low emission for power plants via wet electrostatic precipitators and newly developed demisters: Filterable and condensable particulate matters. *Atmos. Environ.* **2020**, *225*, 117372.
(39) Pan, D.; Qiu, Q.; Zhang, D.; Yang, L. Removal characteristics of SO_3 in the low-low temperature electrostatic precipitator. *Energy Sources, Part A* **2023**, *45* (3), 8092−8103.
(40) Sun, K.; Yan, Y.; Jiang, J.; Deng, L.; Che, D. SO_3 removal efficiency and ash particle flowability of low-low-temperature flue gas systems (LLTSs). *Appl. Therm. Eng.* **2020**, *171*, 115132.
(41) Huang, R.; Yu, R.; Wu, H.; Pan, D.; Zhang, Y.; Yang, L. Investigation on the removal of SO_3 in ammonia-based WFGD system. *Chem. Eng. J.* **2016**, *289*, 537−543.
(42) Wu, Q.; Gu, M.; Du, Y.; Zeng, H. Chemical composition and morphology of particles emitted from a wet flue gas desulfurization (WFGD) system. *Process Saf. Environ. Prot.* **2019**, *124*, 196−203.
(43) Yang, Z. D.; Zheng, C. H.; Li, Q.; Zheng, H.; Zhao, H. T.; Gao, X. Fast Evolution of Sulfuric Acid Aerosol Activated by External Fields for Enhanced Emission Control. *Environ. Sci. Technol.* **2020**, *54* (5), 3022−3031.
(44) Pei, T.; Ma, S.; Zhao, G.; Wang, P.; Song, G.; Mi, C.; Wang, F. Study on the Removal Characteristics of SO3 Acid Mist during the Condensation of Wet Flue Gas. *Ind. Eng. Chem. Res.* **2022**, *61* (10), 3729−3741.
(45) Noppel, M.; Vehkamäki, H.; Kulmala, M. An improved model for hydrate formation in sulfuric acid-water nucleation. *J. Chem. Phys.* **2002**, *116* (1), 218−228.
(46) Vehkamäki, H.; Kulmala, M.; Lehtinen, K. E. J.; Noppel, M. Modelling binary homogeneous nucleation of water-sulfuric acid vapours: Parameterisation for high temperature emissions. *Environ. Sci. Technol.* **2003**, *37* (15), 3392−3398.
(47) Perry, R. H.; Perry, J. H. *Chemical Engineers Handbook*; McGraw-Hill Companies, Inc, 1963.
(48) Shi, Y.; Zhang, X.; Li, F.; Ma, L. Engineering acid dew temperature: the limitation for flue gas heat recovery. *Chin. Sci. Bull.* **2014**, *59* (33), 4418−4425.
(49) ZareNezhad, B. A. General Correlation for Accurate Prediction of the Dew Points of Acidic Combustion Gases in Petroleum Industry. *Pet. Sci. Technol.* **2014**, *32* (16), 1988−1995.
(50) Raj Mohan, B.; Jain, R. K.; Meikap, B. C. Comprehensive analysis for prediction of dust removal efficiency using twin-fluid atomization in a spray scrubber. *Sep. Purif. Technol.* **2008**, *63* (2), 269−277.

https://doi.org/10.1021/acsomega.5c00382
ACS Omega 2025, 10, 19625−19635